2025-01-8454 Published 01 Apr 2025

Effects of Jet Caps on Hydrogen Piezoelectric Injectors for DI Applications: Experiments and 3D-CFD Simulations

Nicolò Pavan Universita di Modena e Reggio Emilia

Giuseppe Cicalese R&D CFD Srl

Luca Gestri Dumarey Flowmotion Technologies SRL

Stefano Fontanesi and Sebastiano Breda Universita di Modena e Reggio Emilia

Marco Mechi and Sara Vongher Dumarey Flowmotion Technologies SRL

Lucio Postrioti Universita degli Studi di Perugia

Giacomo Buitoni STSE SRL

Manuel Martino Universita degli Studi di Perugia

Citation: Pavan, N., Cicalese, G., Gestri, L., Fontanesi, S. et al., "Effects of Jet Caps on Hydrogen Piezoelectric Injectors for DI Applications: Experiments and 3D-CFD Simulations," SAE Technical Paper 2025-01-8454, 2025, doi:10.4271/2025-01-8454.

Received: 05 Nov 2024 Revised: 20 Dec 2024 Accepted: 03 Jan 2025

Abstract

The adoption of hydrogen as a sustainable replacement for fossil fuels is pushing the development of internal combustion engines (ICEs) to overcome the technical limitations related to its usage. Focusing on the fuel injector in a DI configuration, it must guarantee several targets such as the adequate delivery of hydrogen mass for the given operating condition and the proper mixture formation in the combustion chamber playing a primary role in reaching the target performance in H2-ICEs. Experimental campaigns and computational fluid dynamics simulations can be used as complementary tools to provide a deep understanding of the injector behaviour and to drive design modifications in a quick and effective way. In the present work an outward opening, piezo-actuated injector purposely designed to be fuelled with hydrogen is tested on several operating conditions to evaluate its performance in terms of delivered mass flow and jet morphology using the Schlieren imaging technique. To highlight the modification of the jet shape and its interaction with the surrounding air, two different configurations of a single-hole jet caps are placed downstream to the poppet valve. Being one of them optically accessible, some flow features arising inside the cap are seized. 3D-CFD simulations of the tested injector with and without the cap are then performed in transient operation to provide a detailed analysis of the main flow features. Using realistic CAD models, derived from the tested injector and jet caps, together with the poppet lift measurements, the simulations are fully coherent with the tests. A validation study is performed comparing 3D-CFD results with the experiments proving the validity of the developed approach that can be used as a reliable tool to study different injector and injector cap configurations.

Introduction

Driven by legislative demands for a substantial reduction in Greenhouse Gas (GHG) emissions, particularly CO2, in both Europe and the USA, the automotive industry is undergoing a significant transformation to meet these targets. In the EU, the goal is to reduce CO2 emissions from new Heavy-Duty Vehicles (HDVs) based on fleet average emissions by 15% by 2025, 45% by 2030, 65% by 2035, and up to 90% by 2040 [1, 2, 3].

While for passenger cars vehicles full electrification through battery electric vehicles (BEVs) appear to be a viable solution, Hydrogen Internal combustion engines (H2-ICEs) are considered promising to zero the CO2 emissions of Heavy Duty and non-road mobile machinery where high daily range and the remote location of

equipment's limit recharging possibilities. In this sector compromise in driving range, payload capacity, or reliability is not acceptable.

Compared to fuel cells, H2ICEs are tolerant to low purity of hydrogen [4] and can meet similar efficiencies, with peaks beyond 50% with diesel pilot injection, in high load conditions. This, combined with the lower overall cost and higher reliability, make H2-ICEs a more feasible solution [5,6,7].

H2-ICE technology is a short-term solution for reducing emissions, as it requires only minimal modifications to existing engines. These adjustments can be swiftly implemented to produce hydrogen-compatible engines, along with the necessary control software, which can be integrated into the current engine supply chain. This approach offers a significantly lower cost compared to battery electric (BEV) and fuel cell electric vehicles (FCEV).

Hydrogen combustion is carbon-free, but the high temperatures reached during H2 combustion led to formation of NOx emissions from nitrogen oxidation. However, very lean mixtures are tolerated thus allowing to reduce NOx by using selective catalytic reduction (SCR) and exhaust gas recirculation (EGR) allowing to fit current and future regulations [8,9,10].

Both PFI and DI injection systems can be used in hydrogen internal combustion engines. PFI systems are simple from a constructive point of view but show important drawbacks related to backfiring risk and specific performance reduction [11,12]. When adopting DI the above drawbacks can be overcome but issues with mixture preparation could arise.

Two main injection strategies can be employed: Low Pressure Direct Injection (LPDI), with an injection pressure in between 30 and 100 bar rage or High Pressure Direct Injection (HPDI), when injection pressure is higher than 100 bar. The choice between these two strategies strongly influences the complexity of the injection system and the interaction between the injected fuel and the organized flow motion inside the cylinder. HPDI systems are almost mandatory for high performance applications to increase the H2 mass delivered, but they have as a main drawback the decreasing of the exploitable fraction of fuel in the tank, or the need to adopt a compressor which would reduce the overall powertrain efficiency [13]. From the above LPDI strategies are promising if it is possible to ensure high flow rate trough the injector design.

The adoption of hydrogen direct injection systems typically results in supercritical conditions and in the formation of under expanded gas-jets, in both LPDI and HPDI. Under expanded jets have been extensively studied in the literature and are known to produce peculiar flow structures called Mach disks [14,15].

The interaction of under-expanded jets with the organized flow motion within the engine cylinder can significantly impact key parameters, such as penetration length, jet radius, and shape of the plume. The prediction of these jet characteristics is essential for an effective internal combustion engine design and must guide the development of H2 injectors.

In automotive applications, under expanded jets have historically been analysed in compressed natural gas (CNG) engines [16]. However, as the demand to reduce greenhouse gas emissions—especially CO_2—has grown, attention has increasingly focused on characterizing hydrogen jets [17,18].

In this scenario, 3D-CFD simulations allow for an in-depth understanding of injection related phenomena, offering the significant advantage of investigating various injection conditions without requiring complex measurement and expensive experimental campaigns. This technique can be both cost-effective and time-competitive compared to traditional experimental methods if a reliable methodology is developed and then validated.

On one hand, preliminary CFD analysis helps in identifying the most promising technical solutions, providing design guidelines and shortening the development timeline for innovative products like hydrogen injectors. On the other hand, detailed, validated models can be used to investigate complex phenomena and fine details that are difficult to measure directly. However, as the level of detail increases, so does the demand on computational resources, highlighting the need for methodologies that provide essential insights within time and resource constraints.

Despite hydrogen injection is currently a hot topic in the engine field, well established methodologies for the simulations of incoming gas jets from hydrogen injectors are not still available in literature. To reduce uncertainties, simulations validation and sensitivities are commonly carried out modelling the injection process in static vessels and comparing the CFD results with measurements, mainly performed using inert surrogate gases such as Helium.

Kaczmarczyk et al [19] compared CFD results with experiments under different nozzle pressure ratios evaluating the influence of modelling choices such as the equation of state and numerical discretization order on the quality of the results. Reliable results are obtained with the Soave-Redlich-Kwong equation of state and MUSCL scheme at the expense of high computational cost.

Similar sensitivities are performed by the authors in previous studies both in steady-state and transient conditions comparing the numerical results to the experimental data from a single hole LPDI varying both injection pressure and back pressure [20,21]. A low sensitivity of the results to the selected turbulence model is noticed, while improvements are obtained when using real gas equation of state, coupled flow solver and a quite refined mesh in the near nozzle region.

The application of exchangeable injector caps to outward opening injectors is a promising solution to optimize the mixture formation in the combustion chamber allowing to change the gas jets pattern without modifying the injector design. Several studies in literature [22,23,24] explored through numerical simulations the mixture formation with several cap designs (number of holes and distributions), while insights on how the cap influences the injector performance are not provided.

The aim of this paper is to provide a deep analysis of how the application of an injector cap can influence the injector behaviour and the gas jet development. The main flow features inside the cap will be also deepened. To this purpose, a newly developed outward-opening hydrogen injector, both with and without injector caps, is characterized through a coupled experimental and numerical activity.

Experimental data, including needle lift, mass flow rate, and Schlieren imaging, reveal a substantial influence of the injector cap on gas jet evolution within a quiescent vessel. Using this experimental data, a numerical model is developed and validated to accurately replicate the observed effects of the injector cap and to get a deeper investigation of flow characteristics both inside and outside the cap.

Injector Characteristics

In this study, a prototype hydrogen DI injector provided by Dumarey Flowmotion Technologies has been used. While the core body architecture is still under development, an initial learning phase for nozzle and jet cap design is being conducted. The prototype hydrogen injector is derived from a gasoline piezo injector that has been re-designed by enlarging internal flow sections and removing any internal filters. The injector features an outward-opening nozzle configuration with rapid needle displacement and minimal shot-to-shot dispersion. Needle lift can be adjusted by modulating the energy supplied to the piezo actuator, which, in this study, is set to its maximum level.

Two additional mechanical features have been specifically designed for this activity and incorporated into the tool injector:

1. A dedicated removable blocking system enables the rapid test of multiple jet caps variants with the same injector, allowing direct comparison without
   any uncertainties related to part-to-part variability.
2. A special transparent jet cap provides optical access to the jet chamber offering a novel method to compare flow structures between simulations and test.

A preliminary set of CFD simulations and screening DoEs, have been run in steady state conditions to:

- check the static flow rate and pressure distribution inside the tool injector, demonstrating that there is no significant pressure drop through the internal gas flow path allowing the stand-alone simulation of the nozzle in transient conditions
- support the design of the jet caps to be mounted on the tool injector by evaluating the impact on flow rate, pressure field, jet characteristics of the following geometrical parameters:
  - number of flow holes
  - flow holes diameter
  - flow holes taper
  - flow holes elevation angle
  - jet cap chamber height and width

To avoid any geometrical uncertainness due to the manufacturing process of both injector and jet cap, all the tested variants have been measured and the resulting dimensions have been applied to define the corresponding 3D CAD models, ensuring the building of high-fidelity digital twins of the actual ones. Based on the results, several jet caps configurations have been selected and manufactured. For the experimental campaign, 2 exit cross-section levels have been defined: A_Small = 1.767 mm^2 and A_Large = 7.068 mm^2. The larger area has been maintained as a constant across the caps featuring different number of holes, as schematized in Figure 1. The volume of the jet-cap is equal to 494 mm^3.

In addition, to enhance the understanding of the flow established from the nozzle exit down to the jet-cap's flow holes two special optically accessible caps have been designed, one with a single hole and one with 2 holes, maintaining the same total exit cross sectional area as the non-transparent jet cap. The volume of these transparent caps is equal to 592 mm^3, slightly higher than the non-transparent one. Particularly, the distance from the PDI nozzle axis and the vertical walls of this jet-cap is equal to the radius of the internal walls of the non-transparent version. The CAD assembly of the optically accessible caps is reported in Figure 2.

FIGURE 1 Jet Cap with different hole number, total cross section and axis elevation.

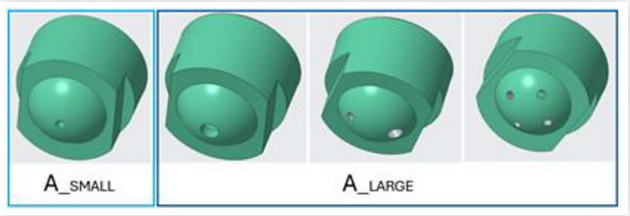

FIGURE 2 Transparent Jet Cap with different hole number, size and axis elevation. "El" indicates the elevation angle.

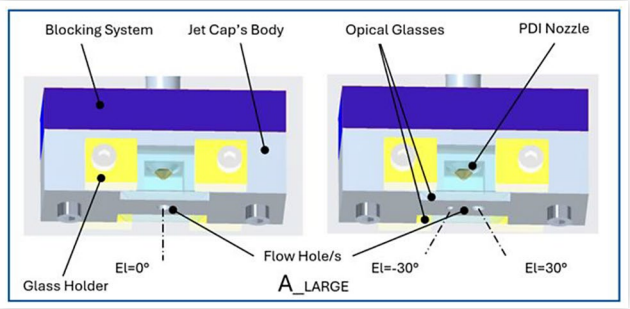

FIGURE 3 JetCap and Transparent JetCap used during experimental campaigns.

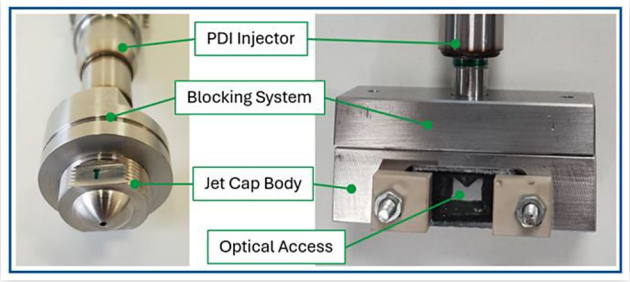

A detailed geometrical characterization of the injectors' nozzle components has been carried out for all the manufactured parts before the assembly phase in the sample lab. Based on these measurements, realistic CAD Models have been created to be used in the CFD simulation study. The same approach has been applied to any variant of the Jet Cap. In Figure 3 a picture showing the actual injector configurations used for the experimental analysis is reported.

Experimental Set-Up

The experimental characterization of the prototype outward opening, piezo-actuated pintle injector designed for hydrogen application is carried out in a range of operating conditions in terms of gas feeding pressure and actuation durations measuring the mean mass/shot, the needle lift time-profile and analysing the evolution of the gas jet in ambient conditions. All the tests are carried out using Helium working fluid, supplied to the injector at ambient temperature. Helium is injected directly into the atmosphere, and hence the ambient pressure is 1 bar and the temperature is 21 °C.

With the developed set-up (Figure 4), the gas feeding and injection pressure/temperature conditions control system are common to all used measurement devices. The test fluid is stored in a cylinder pressurized at 150 bar; a precision mechanical regulator is used to control the injection pressure level at the requested level (in the range 20 to 60 bar for the present test plan) in a 100 cc rail upstream the injector. The rail pressure during the injection event is acquired using a Kistler 4007 piezoresistive sensor; a K-type thermocouple is used to monitor the gas temperature in the rail. Downstream the pressure regulator, a Coriolis-type flow meter (Siemens Mass2100) is used to detect the mean mass flow rate in each operating condition. The injector is actuated by a Dumarey programmable driver using a 170 V peak voltage profile. All the actuation and synchronization signals as long as the signals from the experimental test are respectively produced and acquired by the bench control system based on a proprietary software developed in LabVIEW and on a NI PCIe 6351 signal acquisition/generation board.

FIGURE 4 Schematic of the gas injection systems test bench. Test vessel not shown.

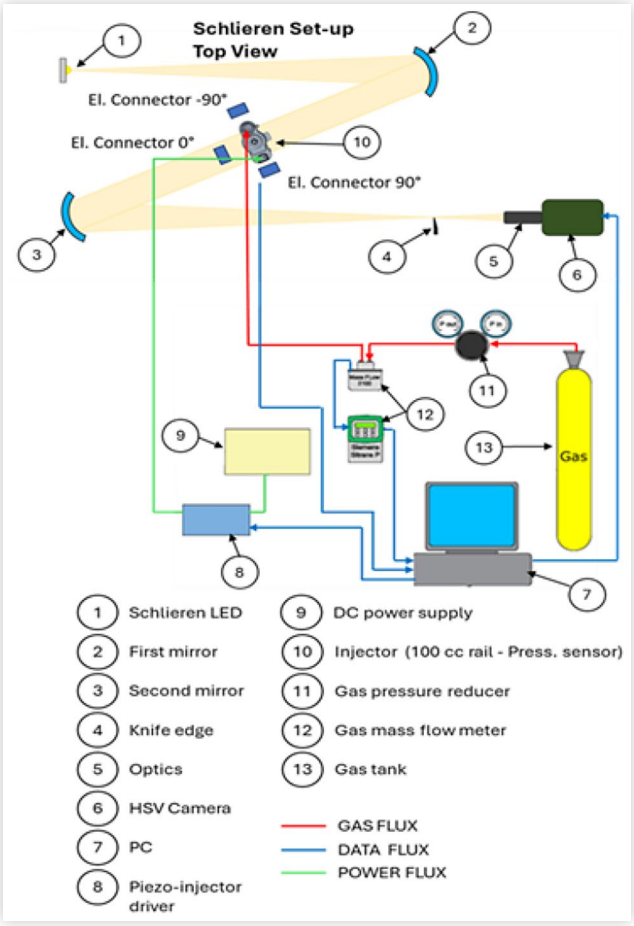

The injector needle displacement during the injection event, used as input for the unsteady CFD simulations, is detected using a Polytec NLV – 2500 laser doppler vibrometer using the procedure described in detail in [25]. For the present setup, the vibrometer laser spot is pointed directly onto the external surface of the injector pintle by 3-axis micrometric positioning system. In the no-cap configuration the gas conical jet emerging from the nozzle leaves a clean central volume in the laser-injector optical path, allowing a relatively easy measurement of the needle lift time-history, for which only the injector body vibrations during the injector event must be accounted for. Conversely, with the axial-hole cap configuration the needle measurement could be possible in principle but the presence of shock-waves due to the gas expansion along the optical path seriously affects the measurement accuracy.

Schlieren imaging [26,27,28] is used to investigate the evolution of the gas jet emerging from the nozzle or from the injector cap in different configurations and operating conditions. As better described in [21], the used Schlieren setup is in Z-configuration (see Figure 4) and allows to follow the jet evolution in a 150 mm-diameter flow field. A high-speed CMOS camera (Phantom Vision Research 7.10) is used to capture the Schlieren videos, operated at

FIGURE 5 Schematic of the gas injection systems test bench. Test vessel not shown.

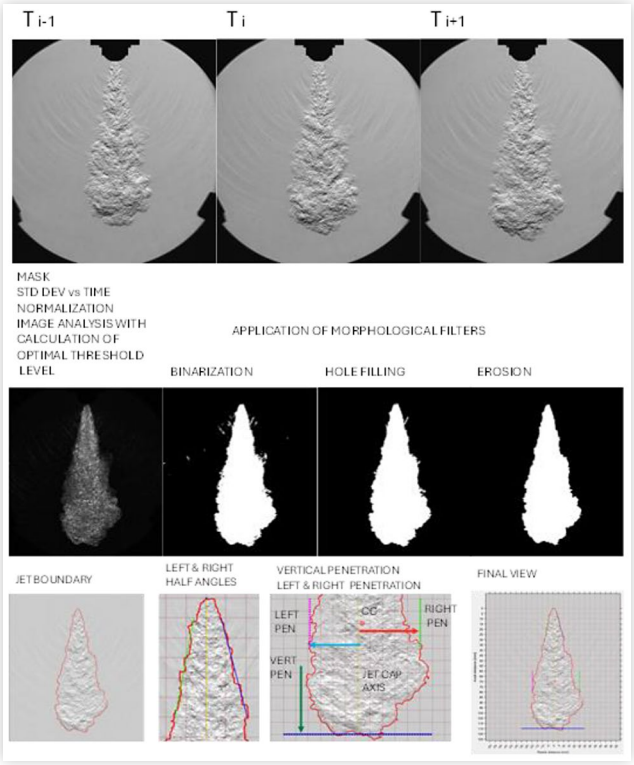

10000 fps (800x880 px) and 100000 fps (250x200 px) respectively for the full flow-field and for the flow evolution just downstream the nozzle. For these two optical configurations, the high-speed camera is equipped with 200-mm and 300-mm Nikkor objectives, respectively. In all conditions, a 1.0 μs exposure time is used to limit the blur-effect is set. The post processing of the imaging, schematized in Figure 5, has been applied to the large view imaging set up (200-mm objective). The detection of the contour of gas is performed, analysing the variation of any pixel of the picture matrix in time domain. Those pixels showing a standard deviation higher than a threshold value are considered as part of the spreading plume. After the binarization morphological filters are applied and the coordinates of the contour derived for the calculation of the jet's characterization metrics. In particular, the cone angles have been calculated 30 mm down to the exit cross section for the configurations with jet cap and 5 mm down to for the configuration with the injector stand alone. Lateral penetration is calculated using a window of 40 mm high and centered on the center of gravity of the jet plume.

Experimental Results

The experimental characterization of the piezo-actuated injector consisted in the application of the above-described methodologies in a wide range of operating

FIGURE 6 Flow curves for the no-cap configuration and different rail pressure levels.

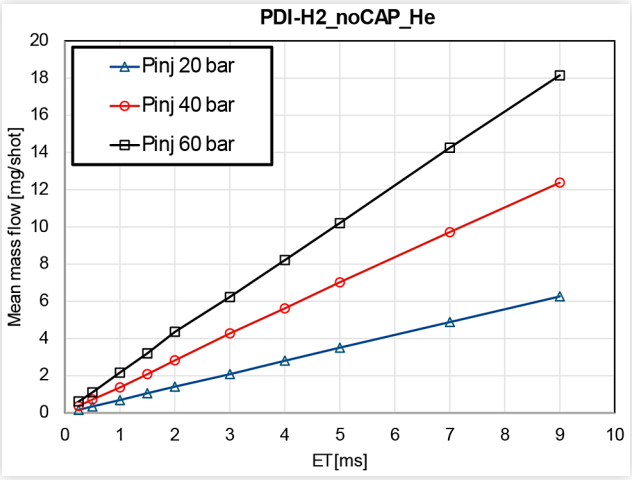

conditions, with feeding pressure among 20 and 60 bar and injector actuation time up to 9 ms. In the same operating conditions additional tests were carried out with the nozzle equipped with caps, designed to guide the gas jet evolution in the volume downstream the nozzle. The present tests are intended to both explore the actual efficacy of the caps and to verify their effects in terms of flow rate depletion.

The mean injected mass per shot produced by the injector in no-cap configuration with different rail pressure levels and energizing times (ET) is reported in the following Figure 6. As can be seen, the obtained trends are almost perfectly linear in a wide range of the actuation time, as expected due to the piezoelectric actuation featuring a very short needle rise time to the fully steady flow condition.

The presence of a cap to actively control the gas jet development in the different zones of the combustion chamber can potentially produce non-negligible effects in terms of pressure downstream the injector nozzle (*i.e.* a pressure increases in the cap) depending on the cap design. Different caps were tested in the present activity, featuring different holes number and size. As an example, in Figure 7 the mean mass per shot obtained with two single-hole caps featuring significantly different hole size are reported. As evident, the jet shape and direction can be actively controlled without having a significant reduction in the flow rate as drawback if the hole geometry is properly designed. The distribution of the same flow area over a higher number of cap holes, obtaining a more uniform fuel distribution in the combustion chamber, is in the present case paid with only a marginal flow rate decrease.

The appearance of the gas jet structure obtained with the nozzle and cap configurations relevant to Figure 7 is reported in Figure 8 for a fully-developed jet timing (1.5 ms from injection start); here the efficacy of the tested caps in controlling the jet development can be appreciated. A marginal reduction of the flow rate has been observed for the 4 holes configuration respect to the

FIGURE 7 Flow curves for different cap configurations with Pinj 60 bar. The effect of different cap configurations can be noticed

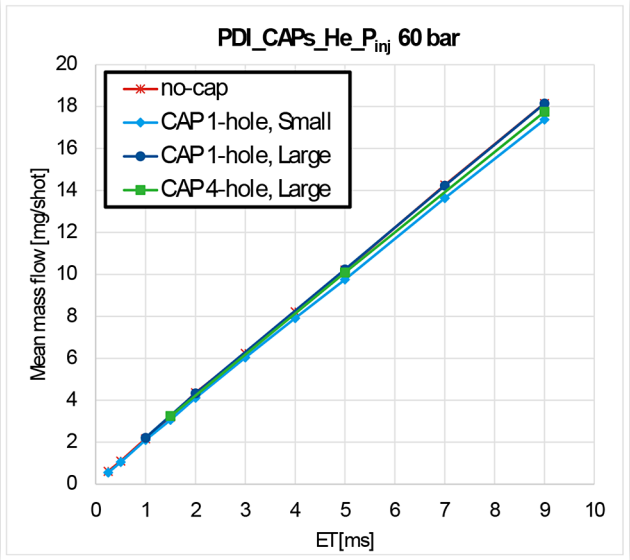

FIGURE 8 Gas jet evolution with different cap configurations. Pinj 60 bar, 1.5 ms after start of injection.

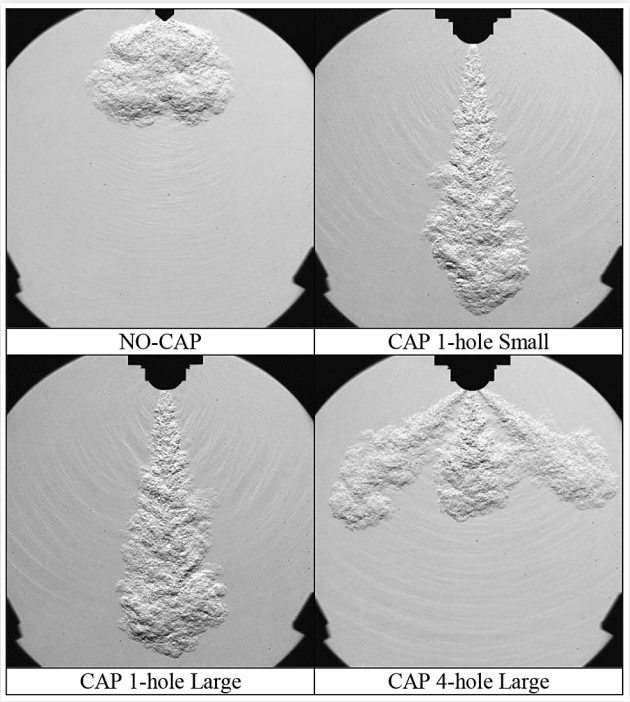

single hole: a higher wall dissipation is expected since the total perimeter of the 4 holes (36.85 mm) is twice the perimeter of the single hole (18.85 mm), and thus the lateral area of the orifices is higher, while the total cross section is the same (7.068 mm^2).

The measurement of the needle lift during the injector actuation is obtained by the above-described laser vibrometer in all the tested operating conditions. In Figure 9 an

FIGURE 9 Needle lift and rail pressure time histories. Pinj 60 bar, ET 0.5, 2 and 9 ms. No-cap configuration.

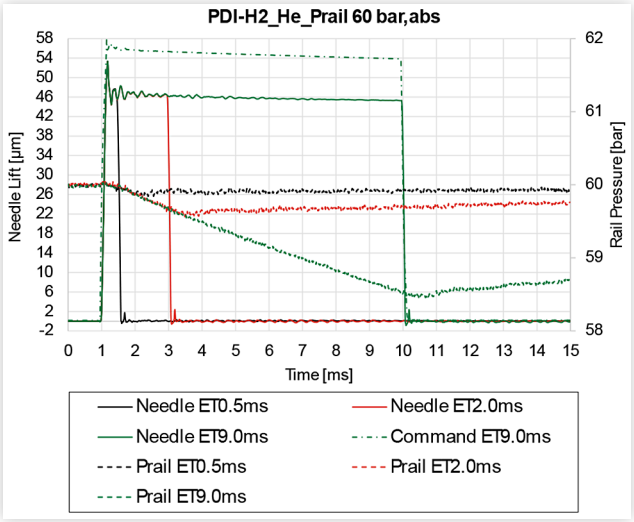

example of the simultaneously acquired trends for the time-histories of needle lift, injector command and rail pressure are reported.

After the driver command start (only shown for the highest injection duration for the sake of the clarity), the needle starts to descend with a delay of about 3 µs and attains its final mean displacement (47 µm for the analysed conditions) in about 180 µs; the initial overshoot to 53 µm is recovered with few oscillations in about 0.3 ms. The displacement of the needle depends on the elongation of the piezo actuator, which is reduced by the reaction forces provided by the needle. These forces consist in a needle spring closing force and an upward pneumatic one acting on the dynamic sealing that is welded on the needle body which grows with the increase of the rail pressure. In the GDI application the lift reduction caused by this phenomenon is managed with a compensation function that increases the energy provided to the piezo stack determining a larger elongation of the actuator. In the present set up, it has been used a fixed energy level for the piezo actuator and with the actual operating conditions in terms of rail pressure an impact on the needle lift is noticed (Figure 10).

Indeed, the final needle displacement is significantly depleted (~4 µm) by the rail pressure level raised from 1 bar (no-flow conditions) to the 60 bar (abs) nominal level. Observing in detail the complete injector opening (Figure 11), the progressive reduction of the obtained needle outward displacement with the rail pressure seems to be mainly originated by an increased initial delay, i.e. by an initially lower acceleration in the first ~20 µs, while in the rest of the process the needle velocity seems to be similar for the different cases.

The displacement of the jet plume contour during the first 100µs of the injection has been investigated for both the configuration without cap and the configuration with the transparent jet cap. In the configuration without cap (Figure 12) a propagation velocity of about 104 m/s

FIGURE 10 Injector needle lift with different rail pressure levels

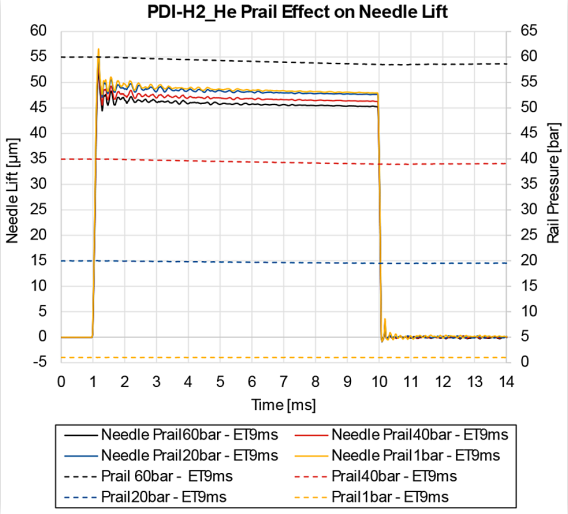

FIGURE 11 Detail of the complete injector needle lift with different rail pressure levels

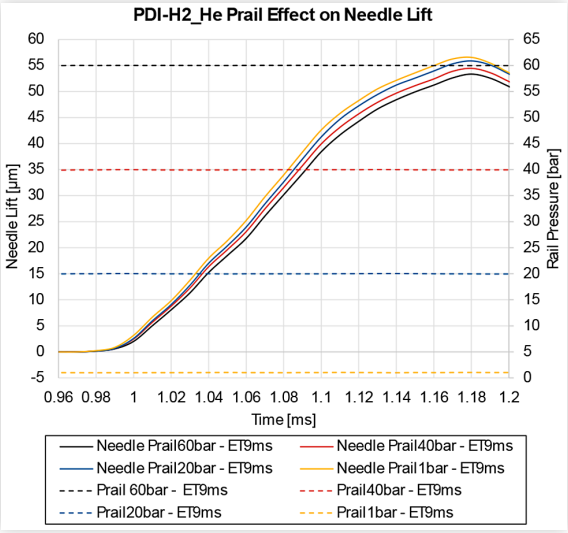

FIGURE 12 Evolution of the gas jet injecting helium in air at atmospheric conditions without caps

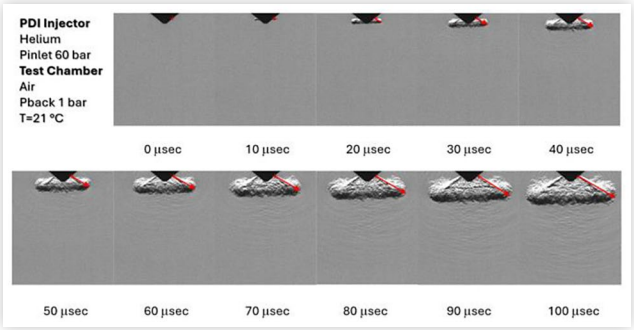

FIGURE 13 Transparent Jet Cap A_Large: evolution of the gas injection inside and outside the jet cap and tracking of the attachment point of gas on the jet cap's walls

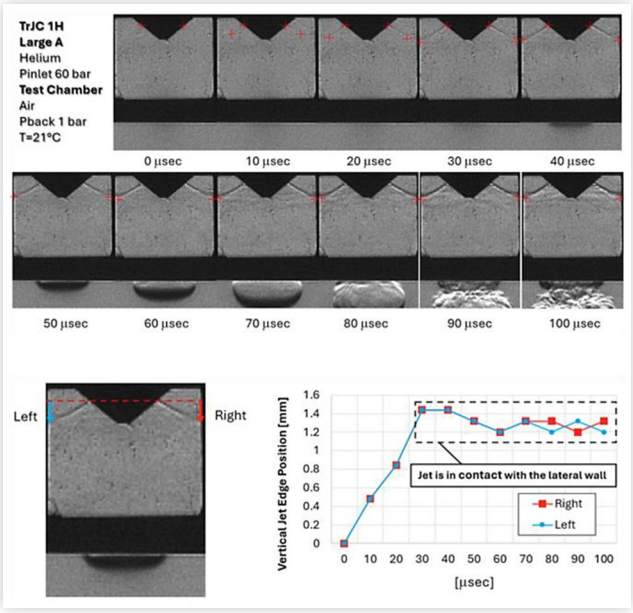

is found. It is important to notice that the calculated velocity is not the velocity of the core of the jet, which is supersonic because of the injection conditions but the average (from a spatial standpoint) velocity of the plume.

The same considerations of the jet evolution inside the cap have been drawn thanks to the use of the transparent jet cap configuration mentioned above. The transparent jet cap shows the evolution of the gas stream inside the cap volume (Figure 13). The border of the jet plume has been tracked from the nozzle exit (t=0 µs) to the attachment point on the jet cap's lateral walls (t=30 µs). The average velocity in this phase is 92m/s. Furthermore, at t=50 µs a gas bubble starts to form at the exit of the jet cap's flow hole and at t=90 µs, a full stream of the gas jet replaces the bubble. The vertical position of the stream attachment point inside the jet cap shows a fluctuation in time coherent with the corrugations that appear on the hollow cone gas distributions below the nozzle tip. The bubble formation and the hollow cone fluctuations might be linked to pressure waves traveling inside the jet cap.

Same phenomenon, in the buildup of the external jet, is observed with the non-transparent version of the jet cap (Figure 14). For this variant, the timing of the events is anticipated of about 10 µs, coherent with the already mentioned lower volume respect with the transparent one.

The experimental results obtained by the application of the above-described methodologies - hydraulic characterization of the injector, simultaneous rail pressure and needle displacement measurement, gas jet spatial evolution by Schlieren imaging – were used to build a detailed portrait of the piezo-actuate prototype injector; further, they were used as input and validation data for the CFD

FIGURE 14 Jet Cap A_Large: evolution of the gas injection outside the JetCap

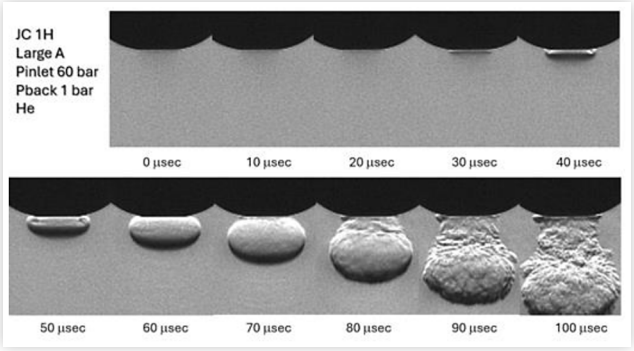

simulation of the injection process described in the following sections.

CFD Methodology

In this paragraph the description of the numerical model developed is reported, with particular attention to the simulation strategy, the adopted mesh and physical models. Simulations are performed with the commercial software Simcenter Star-CCM+ v2402 licensed by Siemens DISW.

Two configurations have been simulated: the first one corresponds to the configuration without cap, and it is called NoCap; the second one corresponds to the configuration with the non-transparent jetcap in the single hole A_Large configuration, and it is called JetCap. The goal of the developed CFD methodology is to obtain a reliable set-up to study the main flow features containing as much as possible the computational cost of the simulations to allow the extensive adoption of CFD simulations in a compatible design timeframe. For this reason, the smallest injection time (equal to 1.5ms) has been selected for the development and validation of the CFD model.

Simulations are performed in a RANS (Reynolds Average Navier Stokes) framework, adopting the Realizable k-ε turbulence model. Exploiting the symmetry of the analysed configurations, a 45° sector, corresponding to 1/8 of the real domain, has been simulated. The numerical domain contains both the injector and the surrounding ambient. Two different domains have been used for the two configurations. For the NoCap case the fluid region is represented by a cylindrical vessel with a radius equal to 100 mm and a length equal to 160 mm, while for the JetCap case the fluid region is represented by a cylindrical vessel with a radius equal to 50 mm and a length equal to 200 mm. A schematic view of the simulated computational domains is reported in Figure 15. The inlet boundary is coloured in pink, the pressure outlet ones are coloured in orange, the symmetry planes are coloured in deep green, and the walls are grey. Furthermore, a detailed view of the cap and of the inlet boundary are

FIGURE 15 Fluid region for the JetCap case (left) and for the NoCap case (right)

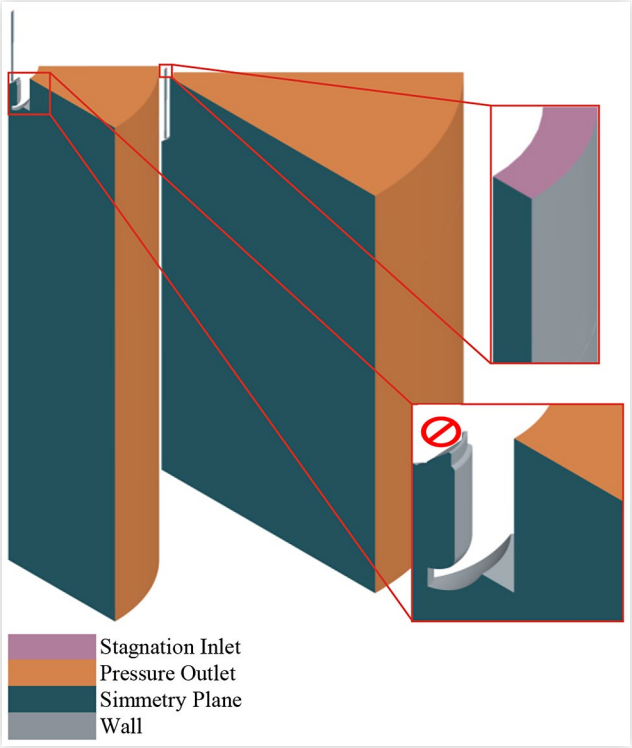

shown. Injector tip has been hidden in the figure for confidentiality reasons.

The case specific ambient dimension is justified by the need to reduce the computational effort and the radically different shape of the jets produced by the two analysed configurations. By optimizing the domain extension, it is possible to keep as low as possible the computational effort without influencing the numerical results applying boundary conditions too close to the jet evolution region. A pressure outlet boundary is considered applying pressure ambient conditions equal to 1.0 bar to the CFD domain borders that don't match the actual ones coupled to 2 symmetry planes. A pressure boundary condition is also applied to the nozzle inlet boundary using the measured rail pressure of 60 bar.

A polyhedral mesh with a base size of 1.0 mm has been used, with local refinements in the proximity of the injector tip and curtain section till to 2.5 µm. Following the choice of adopting two different shapes for the fluid regions in the case with or without the jetcap, also the mesh refinements extensions are different between the two cases but retaining the same level of refinement. In the NoCap case three wide cones are positioned near the needle tip with a cell size equal to 0.03125 mm, 0.0625 mm, 0.25 mm, respectively. On the contrary, on the JetCap case three narrow conical refinements starting from the jet exit section with a cell size equal to 0.125 mm, 0.25 mm, 0.5 mm respectively have been used, to better catch the main phenomena related to jet exit from the injector and from the cap, and jet development inside the vessel. In the outer part of the fluid domain, the mesh

FIGURE 16 Mesh in the two configurations

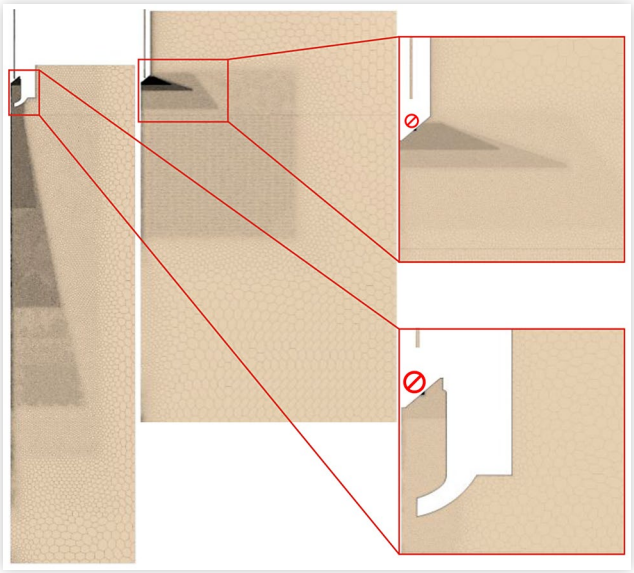

is progressively coarser, till to 4.0 mm on boundaries, to reduce the computational effort in the regions far from the main injection related phenomena.

To ensure a low Reynolds wall treatment with y+ values lower than unity, 10 prismatic layers are applied to the surfaces of needle, injector tip and walls, and to the cap walls. A representation of the mesh in the two cases with detail on the injector tip and jetcap is reported in Figure 16.

The needle lift is treated with a morph and re-mesh strategy. A vertical displacement is applied to the tip according to the experimental measured needle lift law, and the grid is morphed to follow the needle tip movement. Periodic re-meshing events are triggered to ensure an adequate cell quality. A minimum 6.8 μm lift is imposed in closed tip conditions to ensure a good mesh quality in the curtain section when the injector is closed. Table 1 shows the size of the computational mesh in the two cases coupled to the computational effort needed for a complete injection event simulation (2.0 ms) on 208 CPU and a time-step of to 2.5e-7 s.

Regarding the physical models and set-up, particular attention has been paid to the gas models. Considering the peculiar flow characteristics, a real gas approach with the Modified Soave-Redlich-Kwong equation of state has been chosen to represent the flow development. Furthermore, for the same reasons, the coupled flow solver has been used instead of the segregated one. In this way, mass and momentum equations are considered as a system and are resolved simultaneously, providing more robustness and a more realistic description of the flow at the price of a higher computational effort. The specific heat of each species is imposed as a function of temperature through NASA polynomials, while the Sutherland's law is applied for dynamic viscosity. The molecular diffusivity is defined through the kinetic theory starting from dipole momentum, Lennard-Jones characteristic length and energy as a function of temperature and absolute pressure. Regarding the thermal conductivity, the Marthur-Saxena averaging approach has been adopted, while a mass weighted average has been considered for mixture specific heat and dynamic viscosity.

TABLE 1 Computational effort for the two cases simulated

TEST CASE	CELL NUMBER	TOTAL TIME
NoCap	~8.45 M	90 hr
JetCap	~8 M	110 hr

CFD Results

Model Validation

In this section CFD results are analysed and compared to the experimental outcomes. Results are compared in terms of total mass injected, jet penetration and jet width. NoCap and JetCap case are analysed together and against experimental results to verify if CFD results can correctly reproduce the differences between the two configurations and, at the same time, allowing an in-depth understanding of the nozzle flow with and without the cap.

The total mass of gas injected is analysed to check the reliability of the set-up against experimental measurements. In Figure 17 the CFD results and the experimental targets are compared in both the analysed cases. A very good agreement between experiments and CFD is found, with CFD data well inside the experimental error band, evaluated within 1.5% of the measured value. A slight reduction of the injected mass (-5%) is noticed in CFD with the jet cap retaining the same pressure at the inlet

FIGURE 17 Comparison between experimental and CFD mass of helium injected

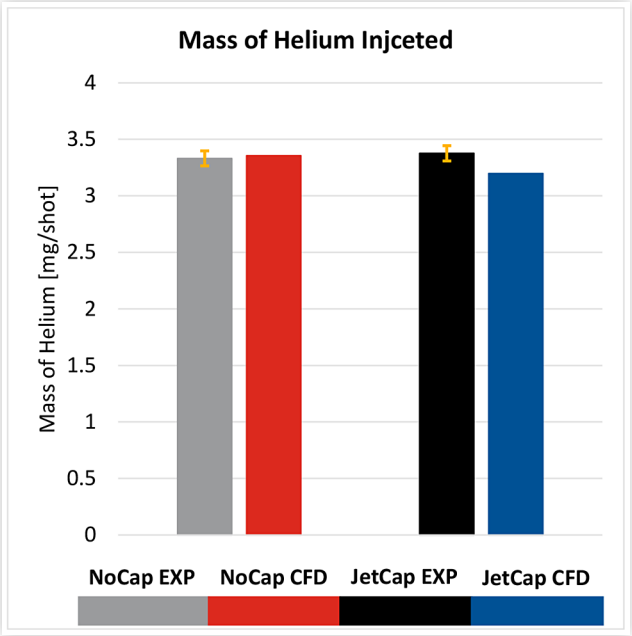

boundary. This is related to the increase of the pressure in the jet cap after the needle opening resulting in a reduction of the pressure rate across the needle (Figure 21). This behaviour, despite expected, is not fully visible from the EXP measurements due to uncertainties on the flow rate measurements (very low variation in the injected mass) also related to the impossibility to retain exactly a constant injection pressure in both cases and during the overall injection event as in CFD. Nevertheless, the small impact of the jet cap adoption on the delivered mass is also confirmed by the CFD results.

In appendix two images (Figure A1, Figure A2) showing the jet evolution in the two cases are reported. Those images show the jet evolution at different instants, comparing experimental schlieren images with CFD density gradient iso-surfaces. Different values of density gradient have been used for the images production (10kg/m^4, 20kg/m^4, 50kg/m^4, 100kg/m^4) with different levels of transparency, in order to achieve a 3D visualization and a deeper representation of the jet inside the vessel. Furthermore, the density gradient iso-surface equal to 20kg/m^4 has been used to calculate jet penetration and jet radius. Particularly, according to experimental set-up, two different cylindrical coordinate system has been used: in the NoCap case, a coordinate system positioned on the bottom surface of the needle tip; in the JetCap case, a coordinate system positioned at the exit section of the cap. In Figure 18 a schematic image showing the penetration and radius calculation method is reported. Both penetration and radius are evaluated considering respectively the maximum axial and radial position in the specific coordinate system.

In Figure 19 a comparison between CFD and experimental penetration is reported. The CFD simulations well reproduce the macroscopic difference between the

FIGURE 18 Penetration and radius calculation method

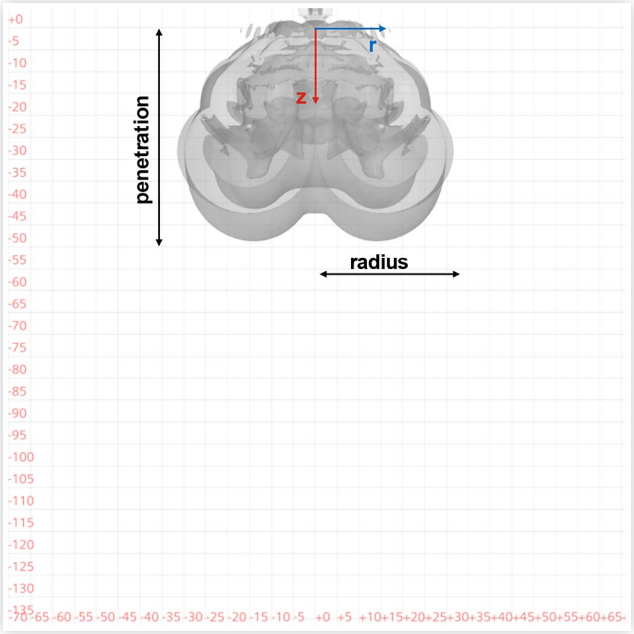

FIGURE 19 CFD and experimental jet penetration. An almost perfect superimposition is visible for the NoCap case, while on the contrary the JetCap one shows a slight overestimation

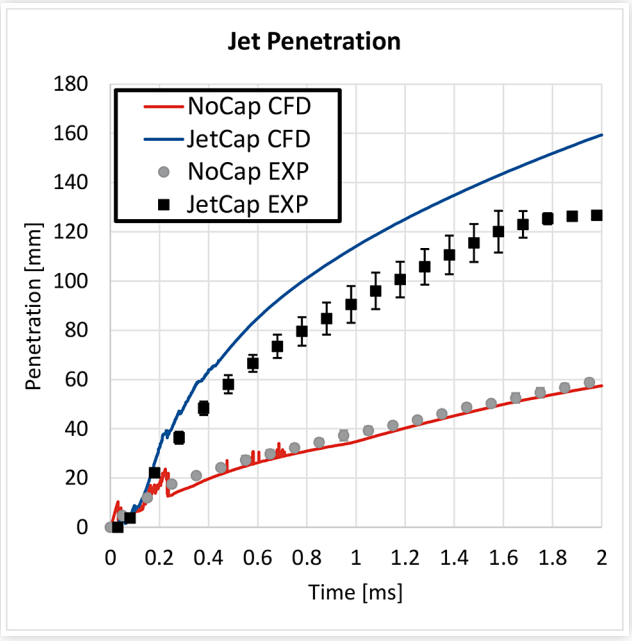

NoCap and the JetCap cases, with a more than double penetration in the case with the jetcap, confirming the trend shown during the experimental campaign and confirming the important difference in the two jets morphology also visible from the appendix. At the same time, a good agreement is found by comparing CFD results with experimental data in the NoCap case, which is almost perfectly superimposed to the experimental trace. In the JetCap case the jet penetration is overestimated above the 2 standard deviation shot-to-shot variation considered. Better results are obtained further refining the grid near the cap hole region, in spite of this, the current setup is selected as the best compromise between accuracy and computational cost.

In Figure 20 a comparison between CFD and experimental jet radius is reported. As can be seen from the graph, CFD simulations well catch the different trend in jet radius between the two configurations, with a wider jet for the NoCap case and a narrower one for the JetCap one. Again, CFD simulations are well aligned with the experimental data for both NoCap and JetCap, with CFD data positioned inside the experimental shot to shot dispersion band width in the JetCap case and just above in the NoCap case. The small discrepancy between CFD and EXP data in the NoCap case can be related again to the mesh, which has been found having a major role in the determination of jet characteristics in poorly wall-guided configurations. Furthermore, also the turbulence model could play an important role, and slight different jet shape could be expected using a different turbulence treatment.

In the NoCap case the jet widens almost suddenly when exiting from the injector, and then it struggles to

FIGURE 20 CFD and experimental jet radius for the two configurations. Experimental data are well matched by the CFD simulations

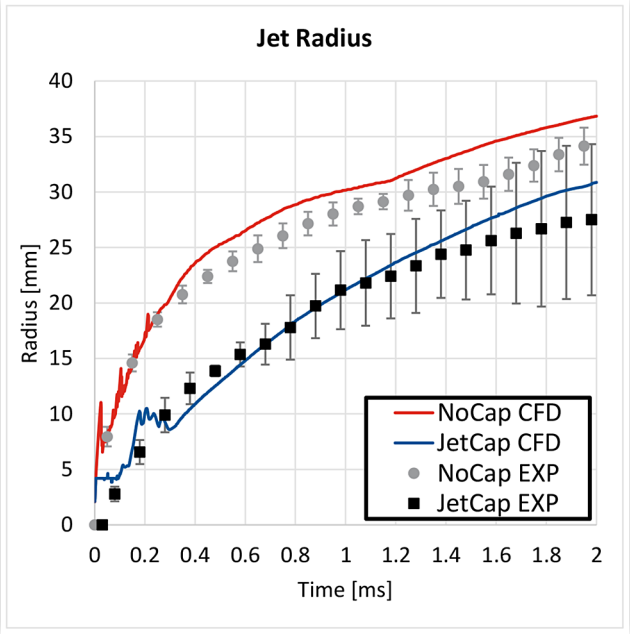

FIGURE 21 Pressure and Temperature evolution inside the cap in the JetCap case

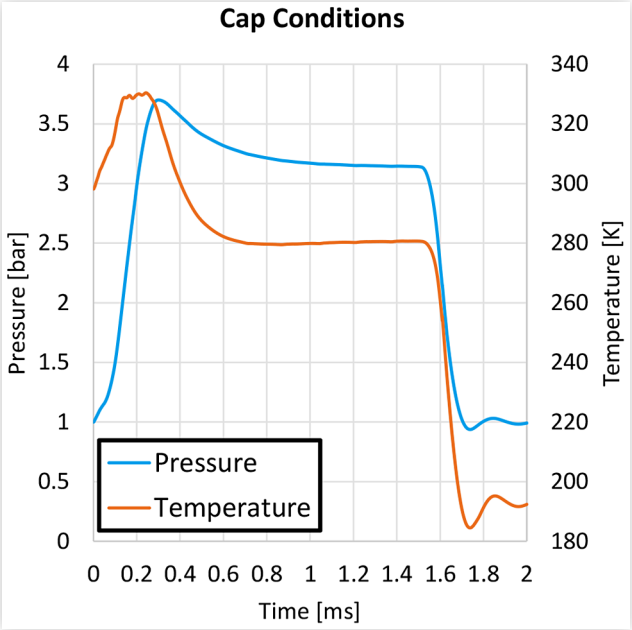

propagate inside the vessel. On the contrary, in the JetCap case the jet has a clear oriented axial direction due to the guide effect produced by the cap hole and it progressively widens as it spreads while moving forward through the vessel.

In the end, through comparison between experimental and CFD data and between the two configurations, the current set-up has proven to be able to reliably match the jet evolution inside the vessel and to correctly represent the different trend between the two configurations, therefore it allows to perform a deeper investigation detailed flow features that cannot be performed with the current experimental set-up.

Flow Characteristics and Details

A deeper investigation of the injection-related phenomena has been carried out and discussed in the current section. At first, the physical condition inside the jet cap during the injection are analysed. In Figure 21 the evolution of temperature and pressure inside the injector cap are therefore reported. In the very first injection phase a fast rise in pressure and temperature is noticeable. Indeed, when the injection starts, the fluid inside the cap is suddenly compressed leading to pressure and temperature rise. In the static injection phase, when the needle is in fully open position, pressure remains almost constant with a value near of about 3.2 bar, while temperature drops to 280 K. This phenomenon is due to a local temperature drop caused by the sudden expansion of the jet at the exit section of the injector, where the high pressure drop produce a supersonic flow leading to the production of shock waves. In the last phase of the injection, pressure and temperature fall due to fluid inertia and positive delta pressure responsible for the injector cap emptying. Particularly, pressure comes back to the ambient condition, while temperature drops below 200K. Pressure evolution inside the cap provides a good explanation to the differences between the two configurations in terms of total injected mass, as already discussed in the previous section. Pressure evolution inside the cap is also responsible for a peculiar flow structure at the hole exit section in the very first phase of the injection, when the cap is in ambient conditions.

A comparison between experimental schlieren images and CFD ones, as density gradient iso-surfaces, is reported at different timings in Figure 22. The production and the evolution of a sort of spherical shaped bubble at the very first phase of the injection produced by the first flow exiting the cap is noticeable from both EXP visualizations and CFD results. This behaviour can be explained by analysing the simulations results and is related to a pressure wave that propagates inside the cap and across the nozzle leading to gas density variation. The generated density gradient, displayed by the Schlieren acquisition, is therefore related to a pressure wave and not to the incoming injected helium from the cap to the vessel that occurs later in time as clearly visible by the pictures in Figure 22.

In Figure 23 Mach disks at the exit section of the injector are reported for both the NoCap and the JetCap case, highlighting a completely different behaviour of the jet comparing the two simulated configurations. In the NoCap case several small Mach disks are visible near the injector, with the jet entering in the ambient with a very high velocity, while on the contrary in the JetCap case only two small disks are visible. Therefore, the presence of the cap walls strongly influences not only the jet

FIGURE 22 Blowing produced in the early phase of the injection inside the cap. Comparison between experimental (the upper one) and CFD images showing, from the top to the bottom, density gradient isosurfaces, density gradient distribution and mass fraction distribution

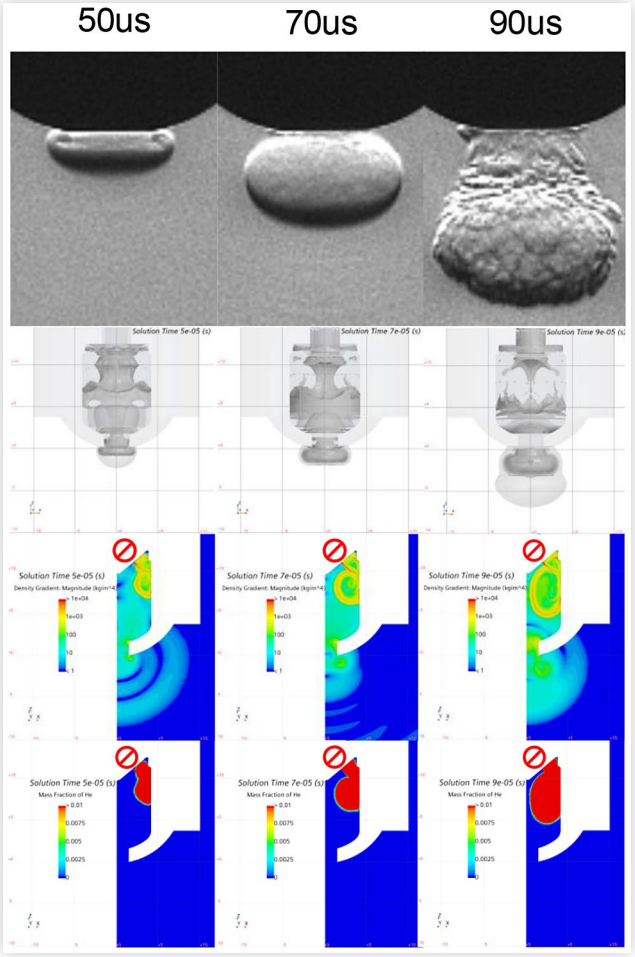

development inside the vessel, but also the jet characteristics around the injector tip.

In the JetCap case the presence of the cap volume produces a pressure rise during the injection, leading to a pressure ratio reduction across the injector with respect to the case without cap. Hence, the outflow velocity from the injector is minor in the JetCap case. Furthermore, the presence of a wall located very close to the tip influences the formation of stationary waves inside the jet, leading to a minor production of structures typical of supersonic flows. The comparison has been carried out by comparing both Mach Number and Velocity Magnitude because the characteristics of the flow inside the cap are different from those of the external ambient and hence also the sonic conditions for the two configurations are different. Particularly, it is interesting to note that for the JetCap case the experimental investigation inside the cap with schlieren imaging technique is really challenging, because after the very first injection phase, the cap is filled with helium and, therefore, it becomes hard to investigate the flow evolution with schlieren imaging, due to the lack of

FIGURE 23 Mach disks produced by the jet exiting from the injector. On the left the NoCap case, on the right the JetCap case

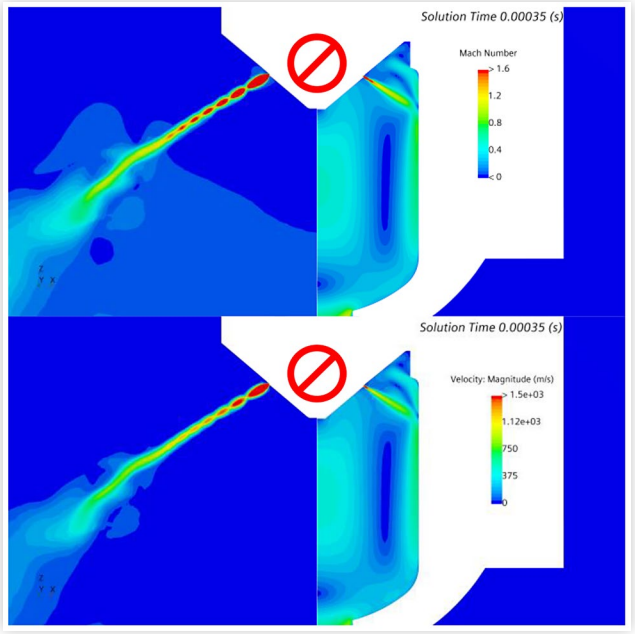

density gradient, while in CFD a detailed study of the flow evolution inside the cap is possible.

In Figure 24, through a larger view, a comparison of the Mach disks in the two configurations is reported showing again significative differences. In the NoCap case the high velocity jet exiting from the injector is subjected to a sudden deceleration when interacting with the

FIGURE 24 Mach disks produced by the stream exiting from the cap in the JetCap case compared to that produced by the NoCap configuration

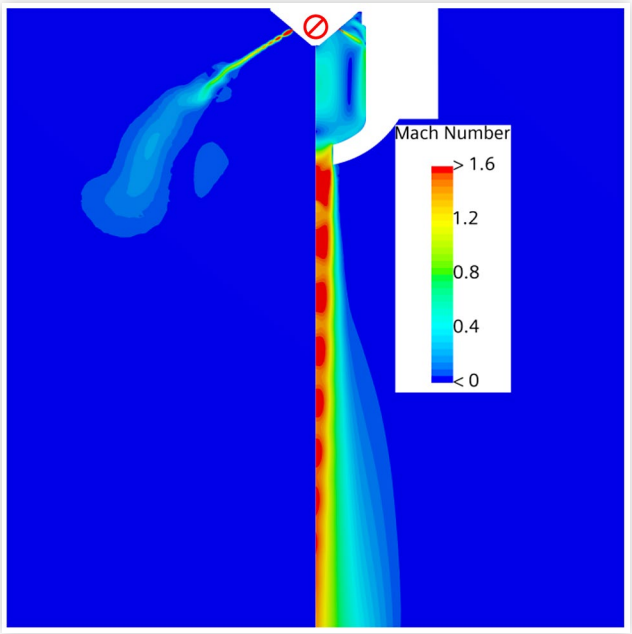

external ambient air, producing an expansion which leads to a wider and shorter jet, and thus Mach disks far from the injector tip are not created. On the contrary, in the JetCap case a high velocity jet exits from the cap with a clearly preferred axial direction, with the formation of several large Mach disks along the jet axis starting from the nozzle exiting section. The jet momentum is therefore increased in the JetCap case due to less jet spreading. The high-pressure ratio between the cap and the external ambient produces a supersonic flow, and therefore phenomena related to under expanded jets are visible through CFD images in the core of the jet, while it would have been difficult to detect this phenomenon through experimental observations because the core of the jet is hidden by the surrounding injected gas.

Conclusions

The joint experimental and CFD analysis has allowed to develop a methodology to deeply investigate the flow characteristics of gas jets from a specifically designed hydrogen injector for engine applications. The flow through the injector was studied and characterized with and without mounting injector caps providing an insight on how the presence of the cap influences the evolution of the gas jet.

Significative differences are found when mounting different jet-caps. Injecting directly into the ambient a wider and relatively short jet is detected; while mounting a cap it is possible to orient the gas jet into the chamber contemporary increasing jet penetration.

The total injected mass has been measured for different rail pressure configurations and for different injection times, showing a linear growth with respect to injection duration thanks to the injector very fast opening and closing transients, that strongly reduce the impact of these phases on the injected mass.

The impact of jet-cap on the injected mass was investigated too, finding a negligible change in the injected mass when applying different cap design with sufficiently high cross-flow section of the nozzles.

The needle lift was also accurately measured, finding a non-negligible impact of the rail pressure on the maximum lift. The measured lift was furthermore an important input for the CFD transient simulations of the injection.

A deeper investigation of the flow development inside the jet-cap was conducted thanks to the use of an optically accessible jet-cap, allowing a detail study of the interactions between gas jet inside the cap and external ambient.

Finally, a CFD methodology was developed and validated on the available experimental outcomes. The simulations can reliably reproduce the differences in terms of gas jets penetration and shape with and without employing an injector cap allowing a deeper analysis of the jet flow characteristics inside the cap. Some details such as the evolution of pressure and temperature in the cap as well the formation of pressure waves after the needle opening can be detailed through CFD that became an important tool to move forward the design of the injector faster reducing the need for time-consuming and costly wide experimental campaigns.

The developed methodology will be further applied to study the gas jet evolution when employing different caps design in terms of shape and hole number, as well as to investigate different injector geometries.

References

1. "Paris Agreement," https://unfccc.int/sites/default/files/english_paris_agreement.pdf.
2. "The Long-Term Strategy of the United States," https://www.whitehouse.gov/wp-content/uploads/2021/10/us-long-term-strategy.pdf.
3. "Reducing CO2 Emissions from Heavy Duty Vehicles," https://climate.ec.europa.eu/eu-action/transport/road-transport-reducing-co2-emissions-vehicles/reducing-co2-emissions-heavy-duty-vehicles_en.
4. Liu, Z., Cai, S., Tu, Z., and Chan, S.H., "Recent Development in Degradation Mechanisms of Proton Exchange Membrane Fuel Cells for Vehicle Applications: Problems, Progress and Perspectives," *Energy Storage and Saving* 3 (2024): 106-152.
5. Sari, R.L., Robles, A.F., Serrano, J.M., and Cleary, D., "Techno-Economic Assessment of Hydrogen as a Fuel for Internal Combustion Engines and Proton Exchange Membrane Fuel Cells on Long Haul Applications," *Int. J. Energy Conversion and Management* 311 (2024). https://doi.org/10.1016/j.enconman.2024.118522.
6. Lad, M.R., Neveu, J.M., and Anoop Krishna, S., "Development of Medium Duty H2 ICE for ON & OFF Highway Application," SAE Technical Paper 2024-26-0170 (2024), https://doi.org/10.4271/2024-26-0170.
7. Sari, R., Shah, A., Kumar, P., Cleary, D. et al., "Hydrogen Internal Combustion Engine Strategies for Heavy-Duty Transportation: Engine and System Level Perspective," SAE Technical Paper 2024-26-0175 (2024), https://doi.org/10.4271/2024-26-0175.
8. Verhelst, S. and Sierens, R., "Hydrogen Engines-Specific Properties", *Int. J. Hydrogen. Energy* 26, (2001) 987-990, Available: www.elsevier.com/locate/ijhydene.
9. Verhelst, S. and Wallner, T., "Hydrogen-Fueled Internal Combustion Engines," *Int. J. Progress in Energy and Combustion Science* 35 (2009): 490-527, doi:10.1016/j.pecs.2009.08.001.
10. Onorati, A. et al., "The Role of Hydrogen for Future Internal Combustion Engines," *Int. J. Engine Research* 23, no. 4 (2022): 529-540, doi:10.1177/14680874221081947.
11. Fontanesi, S., Dalseno, L., and Magnani, M., "Numerical Characterization of Hydrogen Combustion in a High-Performance Engine: Potentials, Limitations, Modelling Uncertainties," *SAE Int. J. Advances & Curr. Prac. in Mobility* 5, no. 3 (2023): 1322-1333, https://doi.org/10.4271/2022-24-0016.

12. Lu, Y., Que, J., Liu, M., Zhao, H. et al., "Study on Backfire Characteristics of Port Fuel Injection Single-Cylinder Hydrogen Internal Combustion Engine," *Int. J. Applied Energy* 364 (2024): 110-123.
13. Vehrelst, S., "Recent Progress in the Use of Hydrogen as a Fuel for Internal Combustion Engines," *Int. J. Hydrogen Energy* 39 (2014): 1071-1085, http://dx.doi.org/10.1016/j.ijhydene.2013.10.102.
14. Crist, S., Glass, D.R., and Sherman, P.M., "Study of the Highly Underexpanded Sonic Jet," *AIAA Journal* 4 (1966): 68-71, doi:doi.org/10.2514/3.3386.
15. Zhao, J., Liu, W., and Liu, Y., "Experimental Investigation on the Microscopic Characteristics of Underexpanded Transient Hydrogen Jets," *Int. J. Hydrogen Energy* 45 (2020): 16865-16873, doi.org/10.1016/j.ijhydene.2020.04.140.
16. White, T.R. and Milton, B.E., "Shock Wave Calibration of Under-Expanded Natural Gas Fuel Jets," *Shock Waves* 18 (2008): 353-364, doi.org/10.1007/s00193-008-0158-6.
17. Anaclerio, G., Capurso, T., Torresi, M., and Camporeale, S.M., "Numerical Characterization of Hydrogen Under-Expanded Jets with a Focus on Internal Combustion Engines Applications," *Int. J. Engine Research* (2023): 146808742211487. https://doi.org/10.1177/14680874221148789.
18. Ruggles, A.J. and Ekoto, I.W., "Ignitability and Mixing of Underexpanded Hydrogen Jets," *Int. J. Hydrogen Energy* 37 (2012): 17549-17560, doi:10.1016/j.ijhydene.2012.03.063.
19. Kaczmarczyk, K.O., Liu, X., Im, H.G., Turner, J.W.G. et al., "Investigation of URANS CFD Methods for Supersonic Hydrogen Jets," SAE Technical Paper 2024-01-2687 (2024), https://doi.org/10.4271/2024-01-2687.
20. Fontanesi, S., Postrioti, L., Magnani, M., Martino, M. et al., "Preliminary Assessment of Hydrogen Direct Injection Potentials and Challenges through a Joint Experimental and Numerical Characterization of High-Pressure Gas Jets," SAE Technical Paper 2022-24-0014 (2022), https://doi.org/10.4271/2022-24-0014.
21. Postrioti, L., Martino, M., Fontanesi, S., Breda, S. et al., "Experimental and Numerical Momentum Flux Analysis of Jets from a Hydrogen Injector," SAE Technical Paper 2024-01-2616 (2024), https://doi.org/10.4271/2024-01-2616.
22. Scalambro, A., Piano, A., Millo, F., Scinicariello, N. et al., "Numerical Analysis of the Hydrogen-Air Mixture Formation Process in a Direct-Injection Engine for Off-Road Applications," *Int. J. Hydrogen Energy* 77 (2024): 1286-1295, doi:10.1016/j.ijhydene.2024.06.193.
23. Mortellaro, F., Tonelli, R., and Medda, M., "Ultra-Lean Mixture Formation and Combustion of a Hydrogen-Fuelled High-Performance DI-SI Engine: an Experimental and Numerical Study", in *THIESEL 2024, Conference on Thermo- and Fluid Dynamics of Clean Propulsion Powerplants*.
24. Sfriso, S., Berni, F., Fontanesi, S., d'Adamo, A. et al., "Combination of G-Equation and Detailed Chemistry: An Application to 3D-CFD Hydrogen Combustion Simulations to Predict NOx Emissions in Reciprocating Internal Combustion," *Int. J. Hydrogen Energy* 89 (2024): 161-176, doi:10.1016/j.ijhydene.2024.09.252.
25. Cavicchi, A. and Postrioti, L., "Simultaneous Needle Lift and Injection Rate Measurement for GDI Fuel Injectors by Laser Doppler Vibrometry and Zeuch Method," *Fuel* 285 (2021): 119021, doi:10.1016/j.fuel.2020.119021.
26. Settles, G.S., *Schlieren and Shadowgraph Techniques: Visualizing Phenomena in Transparent Media* (Springer Science & Business Media, 2001)
27. Panigrahi, P.K. and Muralidhar, K., "Schlieren and Shadowgraph Methods in Heat and Mass Transfer, Springer Briefs in Thermal Engineering and Applied Science," (2012), doi:10.1007/978-1-4614-4535-7_2.
28. Sebastiano Breda, S., Magnani, M., Martino, M., Fontanesi, S. et al., "Experimental and Numerical Characterization of a Single-Hole LPDI Hydrogen Injector: Identification of a Suitable Inert Replacement for Hydrogen Jet Studies," 2024, submitted to Fuel.

Contact Information

Nicolò Pavan, PhD Student
nicolo.pavan@unimore.it
ORCID: 0009-0008-2500-5314
Università di Modena e Reggio Emilia
DIEF - Dipartimento di Ingegneria Enzo Ferrari

Acknowledgments

Sebastiano Breda and Stefano Fontanesi acknowledge European Union-Next generation EU through the "PIANO NAZIONALE DI RIPRESA E RESILIENZA (PNRR) – MISSIONE 4 COMPONENTE 2, "Dalla ricerca all'impresa" INVESTIMENTO 1.4, (CN00000023). In the context of the "Sustainable Mobility Center (Centro Nazionale per la Mobilità sostenibile – CNMS)" – Spoke 12 – Avviso MUR 3138/2021 modificato con DD 3175/2021.

The authors also acknowledge Nicola Boscolo and Alessandro Luschi of Dumarey Flowmotion Manufacturing Team, and Marco Rossi of RTM

Definitions/Abbreviations

BEV - Battery Electric Vehicle
CAD - Computer Aided Design
CFD - Computational Fluid Dynamics
DI - Direct Injection
DoEs - Design of Experiments
EGR - Exhaust Gas Recirculation
EI - Elevation Angle
ET - Energizing Time
EXP - Experimental
FCEV - Fuel Cell Electric Vehicle
GHG - Green House Gases
H2ICE - Hydrogen Internal Combustion Engine
HDV - Headvy Duty Vehicle
HPDI - High Pressure Direct Injection

ICE - Internal Combustion Engine
LPDI - Low Pressure Direct Injection
MUSCL - Monotonic Upstream-centered Scheme for Conservation Laws
NOx - Nitrogen Oxides
PFI - Port Fuel Injection
RANS - Reynolds Average Navier-Stokes
SCR - Selective Catalytic Reduction

Appendix

FIGURE A1 Comparison between experimental and CFD jet shape for the NoCap case

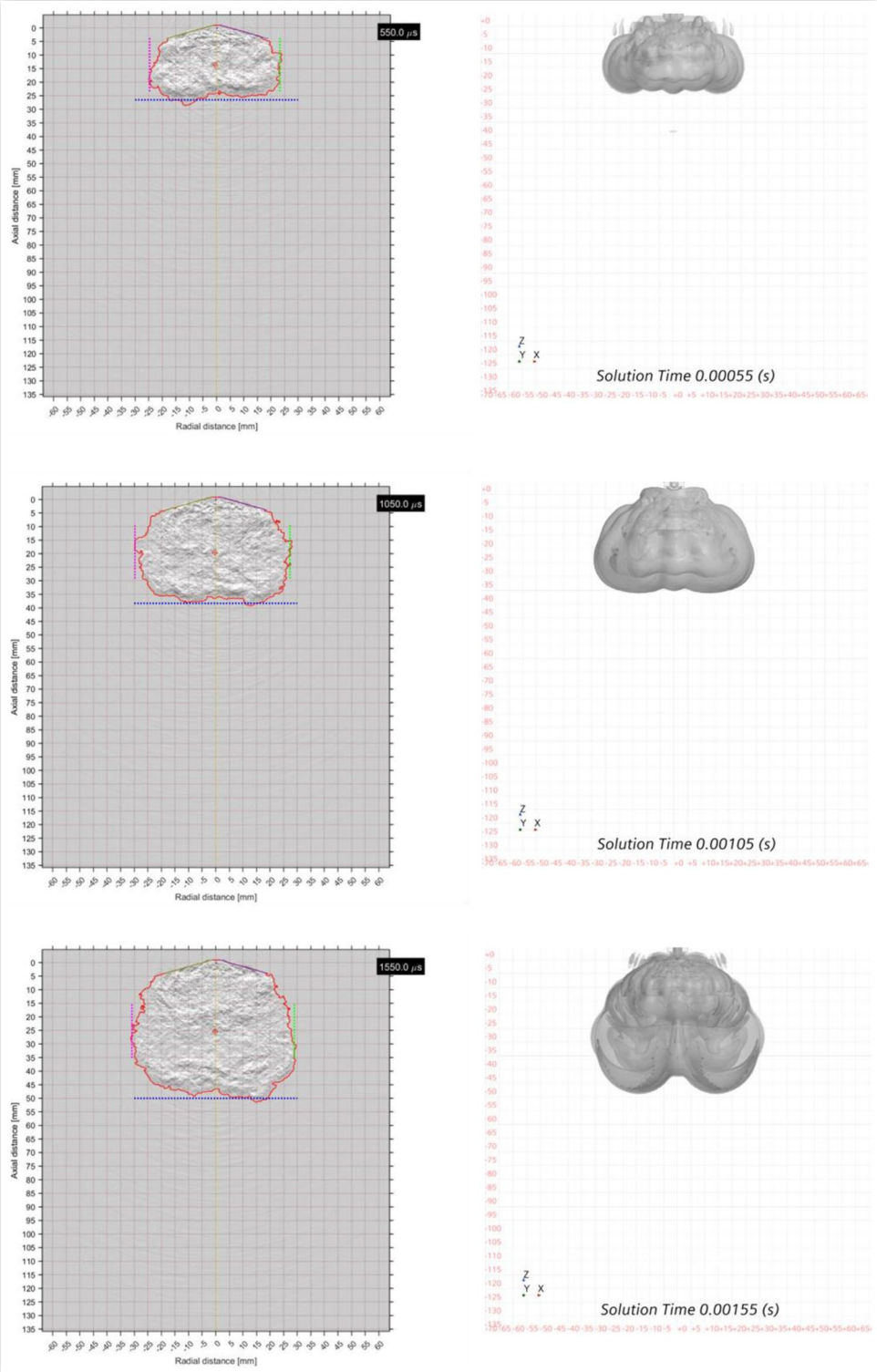

FIGURE A2 Comparison between experimental and CFD jet shape for the JetCap case

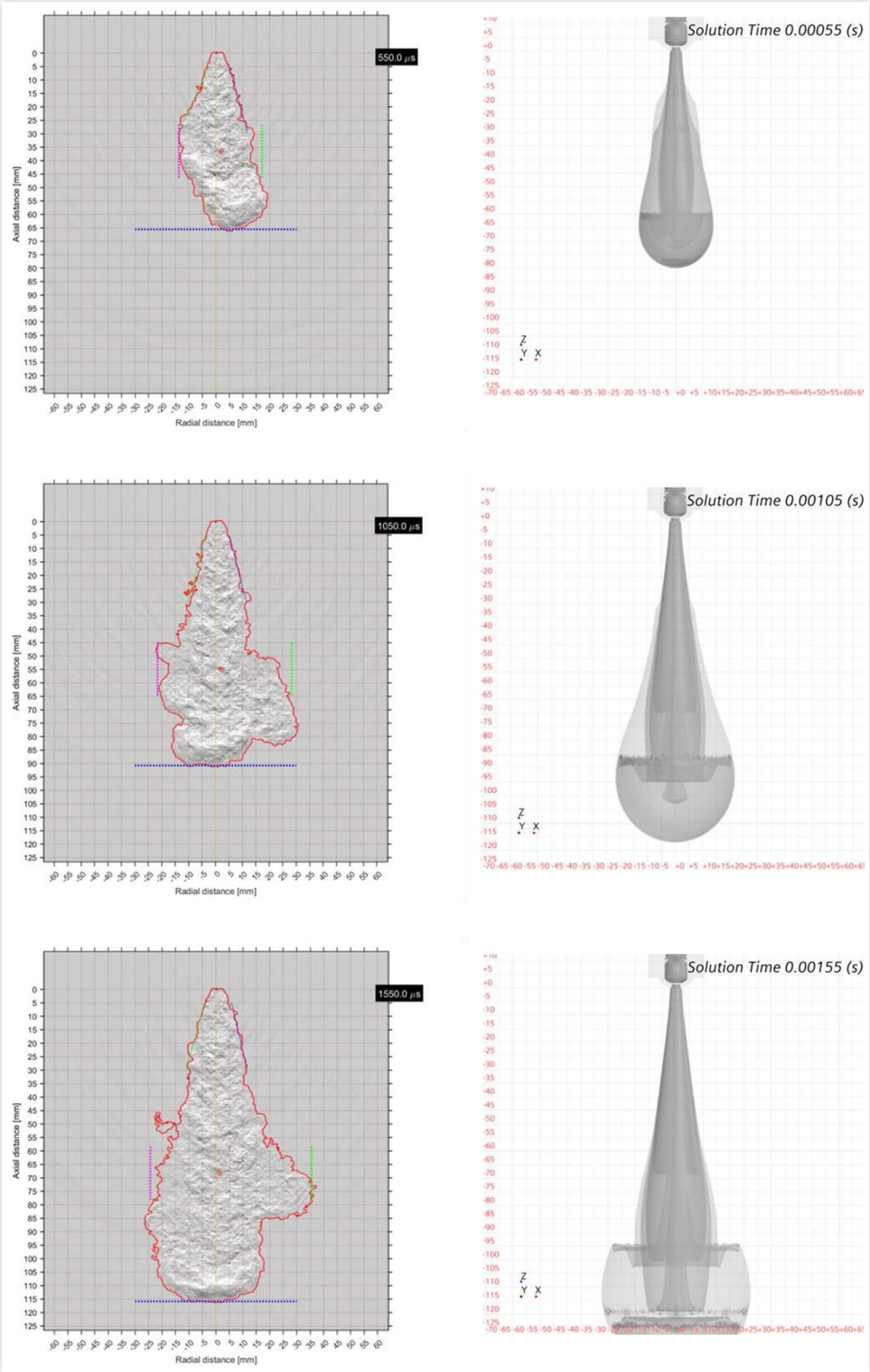

ISSN 0148-7191